

Active vibration control of a gyroscopic rotor using experimental modal analysis

Jens JUNGBLUT*, Christian FISCHER, and Stephan RINDERKNECHT

Institute for Mechatronic Systems, Technical University Darmstadt, 64287, Germany

Abstract. A gyroscopic rotor exposed to unbalance is studied and controlled with an active piezoelectrical bearing. A model is required in order to design a suited controller. Due to the lack of related publications utilizing piezoelectrical bearings and obtaining a modal model purely exploiting experimental modal analysis, this paper reveals a method to receive a modal model of a gyroscopic rotor system with an active piezoelectrical bearing. The properties of the retrieved model are then incorporated into the design of an originally model-free control approach for unbalance vibration elimination, which consists of a simple feedback control and an adaptive feedforward control. After the discussion on the limitations of the model-free control, a modified controller using the priorly identified modal model is implemented on an elementary rotor test-rig comparing its performance to the original model-free controller.

Key words: modal analysis; active vibration control; piezoelectrical bearing.

1. INTRODUCTION

Rotating machines build the foundation of our modern world. They can be found in many different applications such as DC-motors, wind turbines and jet engines. The used rotors are always subject to unbalances which lead to an excitation of the rotor and the surrounding structure. The resulting vibrations cause audible noise and reduce the life span. Lightweight structures are especially sensitive to these vibrations and can show large displacements in resonances, which can cause a total failure of the system. Rotors are balanced in order to reduce the unbalance excitation and thus the vibration. This is achieved by adding or removing rotor mass. If the precision of the passive balancing is not sufficient or the unbalance changes during the operation, for example due to dust, active systems can be used to enhance the vibration reduction. Furthermore, active systems can stabilize the rotor allowing to extend the safe operating range. While active magnetic bearings are mainly used to support a rotor with minimal friction, active piezoelectric elements can be used to support the bearings of heavy rotors due to their high stiffness. Piezo supported bearings allow a fail-safe support in case of a blackout. The actuators can manipulate the rotational axis of the rotor dynamically and change its dynamic behaviour. The first to implement such an active piezo supported bearing was Palazzolo [1]. He used a simple PD-controller to verify functionality of the novel bearing concept over a 30 hour endurance-test. Different research groups picked up the idea and implemented different controllers to enhance the vibration reduction. Model-free feedback controllers such as PDT1 [2] and integral force feedback (IFF) [3] mainly

reduce vibrations in the resonances because they increase the damping of the system. The implemented model-based control approaches such as LQR [4], μ -synthesis [5] and gain scheduled H_∞ -control [6] show a better performance but require more effort for implementation. However, there will always be remaining vibrations since the feedback loop needs a controller input in order to eliminate vibrations. The use of a feedforward or an adaptive feedforward control can overcome this problem. Li [7] implements the filtered-x least mean squares algorithm (FxLMS) to eliminate gear vibrations. The FxLMS is suited well for this task because of the narrow-banded nature of the disturbance which is also the case for unbalance excitation. Suzuki [8] combines a H_∞ -controller with a feedback controller to enhance the vibration reduction. The combination of a feedback controller which takes care of transient vibrations and an adaptive feedforward controller for eliminating the unbalance excitation yields the best vibration reduction results which can be concluded from the work of Lindeborn [9] and Schittenhelm [10]. While Lindeborn combines IFF and the FxLM, Schittenhelm compares the combination of a PD-controller and the FxLMS with a combination of LQG and FxLMS where both combinations show nearly the same performance concluding that a simple model-free feedback controller is sufficient. Finally, Heindel [11] presents a model-free control approach which is based on a combination of IFF and an adaptive feedforward controller. He proves the stability of the controller in the continuous time domain where the controller is always stable.

The approach in this paper leads to an extension of the algorithm presented by Heindel, showing its limitations for implementation on a real system. The system is modelled in a first step. While most publications rely on finite element models, the presented model is identified using experimental modal analysis. A model-free control approach is derived after the system

*e-mail: jungblut@ims.tu-darmstadt.de

Manuscript submitted 2021-03-22, revised 2021-06-09, initially accepted for publication 2021-06-18, published in December 2021

identification and the limitations are discussed. After comparing the experimental results of the model-free control to the corresponding model-based control, a conclusion is presented.

2. MODAL MODEL

Subject of this paper is the system identification and control of the rotor system depicted in Fig. 1. The test-rig has one active bearing plane (Bearing 1) with two actuators allowing to shift the rotor in the spanned y, z -plane. The rotor rotates with the rotor speed $\bar{\Omega}$ into the negative x -direction.

Figure 2 shows the signal flow of the test-rig. The bearing forces $\tilde{F}_{L,y}$ and $\tilde{F}_{L,z}$ of Bearing 1 are measured in the y - and z direction respectively. After filtering the signals with a first order Butterworth high-pass filter, which has the cut-on frequency 1 Hz, the signals are combined to a complex signal $F_L(t) = \tilde{F}_{L,y}(t) + i\tilde{F}_{L,z}(t)$ which hereinafter is referred to as the bearing force. This step is crucial for the later presented control approach since we can easily distinguish the forward and backward whirl and correct the phase of the complex signal throughout a multiplication with a complex number. Analogously, the

displacements $\tilde{r}_{w,y}$ and $\tilde{r}_{w,z}$ of Disc 1 are measured and combined. An incremental encoder is used to measure the instantaneous angle of the rotor φ . The angle is used to subtract the runout of the rotor from the measured displacement so that in theory $r_{w,y}(\bar{\Omega} = U_a = 0, \forall \varphi) = r_{w,z}(\bar{\Omega} = U_a = 0, \forall \varphi) = 0$ is fulfilled. The piezo actuators in y - and z -direction are supplied by the voltages $U_{a,y}$ and $U_{a,z}$ respectively. Both voltages are combined to the complex signal $U_a = U_{a,y} + iU_{a,z}$ which equals the sum of the complex controller output voltage U_c and the separate voltage U_n which is later used for the system identification.

In this paper we aim to eliminate the bearing force F_L . Thus, we require the transfer function $H_F = \mathcal{F}\{F_L\} / \mathcal{F}\{U_a\}$ for active control of the system where the operator $\mathcal{F}\{\}$ represents the Fourier-transformation. This relation needs more explanation since our time signals are complex, as well as the signal in the frequency domain. Under the assumption of a linear system, the relation in the frequency domain is given by

$$\begin{pmatrix} \mathcal{F}\{F_{L,y}\} \\ \mathcal{F}\{F_{L,z}\} \end{pmatrix} = \begin{bmatrix} H_{yy} & H_{yz} \\ H_{zy} & H_{zz} \end{bmatrix} \begin{pmatrix} \mathcal{F}\{U_{a,y}\} \\ \mathcal{F}\{U_{a,z}\} \end{pmatrix}, \quad (1)$$

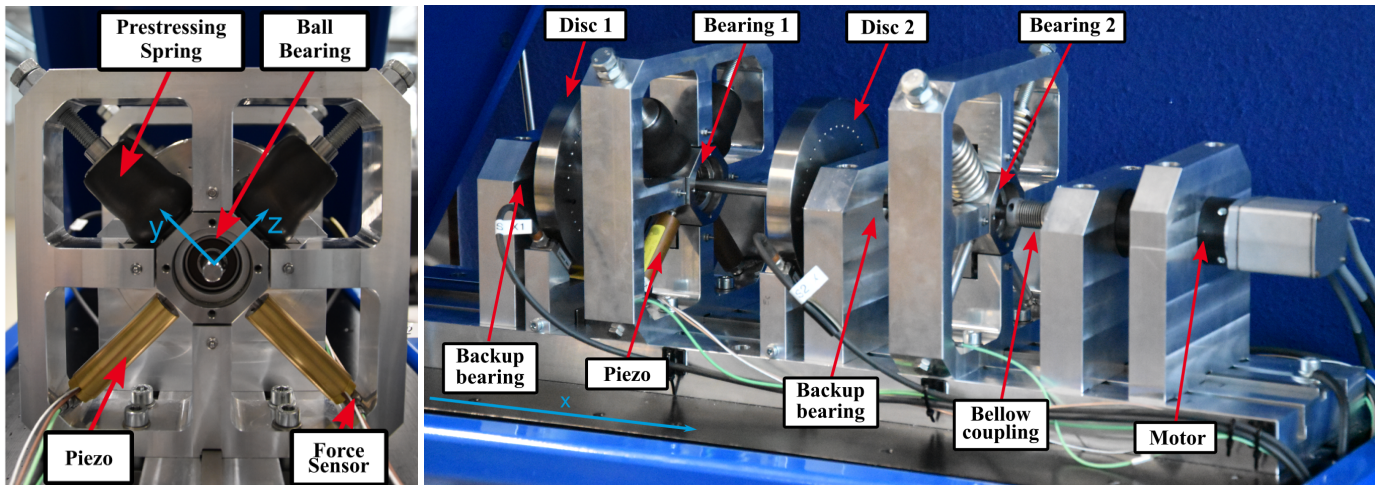


Fig. 1. The test-rig comprises two discs mounted on the shaft with clamping-sets. The test-rig has one active plane (Bearing 1) with piezo actuators prestressed with springs

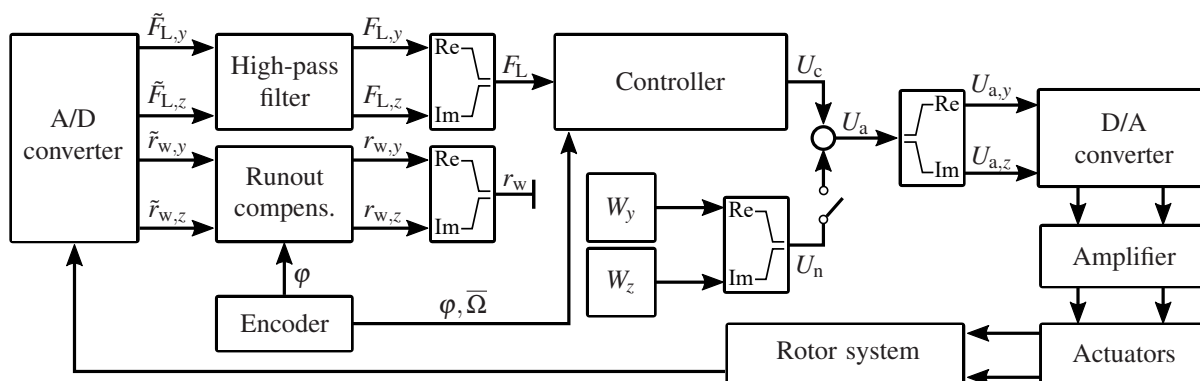


Fig. 2. Signal flow of the test-rig. The bearing forces $\tilde{F}_{L,y}$ and $\tilde{F}_{L,z}$ of Bearing 1 and the displacements $\tilde{r}_{w,y}$ and $\tilde{r}_{w,z}$ of Disc 1 are measured. $\bar{\Omega}$ is the rotor speed and φ the instantaneous rotor angle. U_c is the complex time signal of the control voltage, U_n the voltage from white noise. $U_{a,y}$ is the real valued voltage of the actuator pointing in y -direction and $U_{a,z}$ from the one pointing in z -direction

where Ω represents the excitation frequency. This relation does not allow a complex combination as mentioned above in general. However, if the bearings and the rotor are isotropic, the relations $H_{yy} = H_{zz}$ and $H_{yz} = -H_{zy}$ apply, where the latter one represents the skew-symmetric coupling caused by gyroscopic effects. We can rearrange Eq. (1) under the assumption that the rotor and its bearings are isotropic to

$$\begin{aligned} \mathcal{F}\{F_{L,y}\} + i\mathcal{F}\{F_{L,z}\} &= (H_{yy} - iH_{yz})(\mathcal{F}\{U_{a,y}\} + i\mathcal{F}\{U_{a,z}\}) \\ \mathcal{F}\{F_L\} &= H_F \mathcal{F}\{U_a\} \end{aligned} \quad (2)$$

since the Fourier-transform is a linear operator. The transfer function $H_F = H_{yy} - iH_{yz}$ links the Fourier-transformations of the complex time signals $F_L(t)$ and $U_a(t)$ showing that we can use the same identification process as for real time signals. The transfer function is in general not point symmetrical $H_F(\Omega, \bar{\Omega} \neq 0) \neq H_F^*(-\Omega, \bar{\Omega} \neq 0)$ due to the presence of gyroscopic effects yielding different transfer functions for negative and positive frequencies. This makes it simple to separate forward whirl and backward whirl vibrations. However, the assumptions imply that a forward whirl excitation causes a forward whirl response only and the other way around for a backward whirl excitation. This approach is not suited if a forward whirl excitation causes a forward and backward whirl response as it is the case for non-isotropic bearings.

We need to define the structure of the transfer function for the later identification process. We take the usual approach by separating the function into modes based on the eigenvalues λ_n of the systems. The challenging part here is that the eigenvalues are a function of the rotor speed $\bar{\Omega}$. The eigenvalues can be separated into forward and backward whirl modes since we are using complex time signals and they do no longer appear as conjugate complex pairs because of gyroscopic effects.

We separate the eigenvalues into imaginary and real part which allows for a simpler numerical identification of the parameters. Analogous to the structure of the roots of the characteristic equation presented by Vervisch [12], we approximate the imaginary part using the function

$$\Im\{\lambda_n\} = \omega_n \approx w_{n0} + w_{n1}\bar{\Omega} \pm \sqrt{w_{n2}^2 + w_{n3}\bar{\Omega} + w_{n1}^2\bar{\Omega}^2} \quad (3)$$

with $\omega_n, w_{ni} \in \mathbb{R}$, which represents an undamped eigenfrequency ω_n of the system. Note that \pm indicates two possibilities of which only one is true for each eigenvalue. The real part is approximated using

$$\Re\{\lambda_n\} = -D_n\omega_n \approx -\omega_n(d_{n0} + d_{n1}\bar{\Omega}), \quad D_n, d_{ni} \in \mathbb{R} \quad (4)$$

where D_n represents the modal damping. The parameters d_{ni} and w_{ni} have to be identified and are not directly related to mechanical system properties. Equation (4) has a structure which is analogous to a Jeffcott-rotor with internal damping.

We chose the trial function

$$H_F(\Omega, \bar{\Omega}) = \left\{ H_{F0} + \sum_{n=1}^{n_M} V_n \frac{i\Omega}{i\Omega - (i\omega_n - D_n\omega_n)} \right\} e^{-i\Omega\tau} \quad (5)$$

to model the transfer function for a base excitation of the piezo actuator where H_{F0} represents the static response, which is mainly caused by the prestressing springs and the bellow coupling, V_n the modal residual and n_m the number of considered modes. A delay-time τ is used to cover the delay caused by the power electronics, sensors and the time-discrete real-time system.

3. SYSTEM IDENTIFICATION

The first step of the system identification is the estimation of the frequency transfer function H_F which will then be used for fitting. The rotor was operated at nine constant speeds $\bar{\Omega}$ (0, 1000, 2500, 4000, 5000, 7000, 8000, 9000, 10 000 rpm) while exciting it with a noise-burst with an 80% duty cycle for 20 seconds. The noise w_n was applied throughout two white noise blocks in MATLAB SIMULINK with the same seed, meaning that $W_y(t) = W_z(t) = w_n$. Each measurement was performed 25 times. Additionally, IFF was used during the entire operation of the system because of the presence of internal damping which could lead to an exponential rise of the vibrations as can be seen in Fig. 5. This yields the advantage that the closed-loop transfer function

$$H_{Fc} = \frac{\mathcal{F}\{F_L\}}{\mathcal{F}\{U_a\}} \quad (6)$$

can be estimated which is more relevant for the later control approach than the open-loop transfer function H_F . No adaptive feedforward control is used during the identification process. The open-loop transfer function can be computed from the closed-loop transfer function using Eq. (8) since the transfer function of the IFF-controller is known.

Figure 3 shows the estimated closed-loop transfer function H_{Fc} together with the fit. Negative frequencies correspond to the forward whirl and positive frequencies to the backward whirl. Even-orders of the rotor speed have been cut out. The coherence is very poor at zeros due to the low response but acceptable at the other frequencies.

In the second step, the eigenfrequencies Eq. (3) are fitted with non-linear regression using the Levenberg-Marquardt algorithm. The modal residuals V_F are computed afterwards by applying a weighting for different frequency ranges, with a focus on the operating range between -170 and 170 Hz, guessing an initial value for the modal damping and performing a linear regression. Finally, the damping and the modal residual are optimized together by using the Levenberg-Marquardt algorithm for non-linear regression of the weighted least-mean-square problem.

The fit is in good agreement with the estimated transfer function excepted for the phase at the zeros of the second forward and backward resonances. The real part of the zero at around 130 Hz at a rotor speed of 10 000 rpm is positive while the zero of the fit remains a negative real part. This causes the phase to fall in the estimation but to rise for the fit. The backward whirl resonance here originates at 230 Hz for $\bar{\Omega} = 0$ where the phase increases in the zero before the resonance. The phase decreases in the zero before the resonance starting at $\bar{\Omega} \approx 9000$ rpm. The presented model cannot represent such a behaviour because

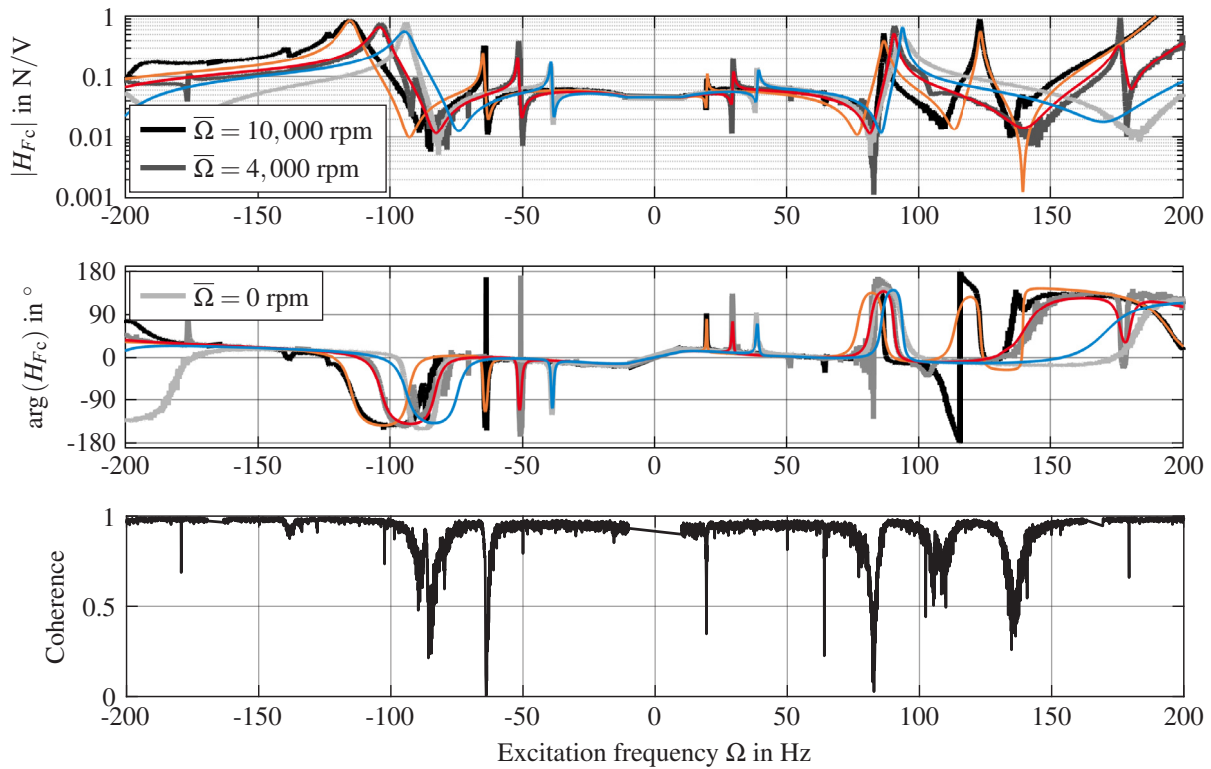


Fig. 3. Estimated closed-loop transfer function H_{Fc} for three stationary rotor speeds together with the fitted modal model with $V_F = \text{const}$. The blue, red and orange line correspond to the fits at 0, 4000 and 10 000 rpm respectively. Negative frequencies correspond to the forward whirl and positive frequencies to the backward whirl since the rotor rotates into the negative x -direction. The legends are shared among all plots. The coherence belongs to the measurement at 10 000 rpm

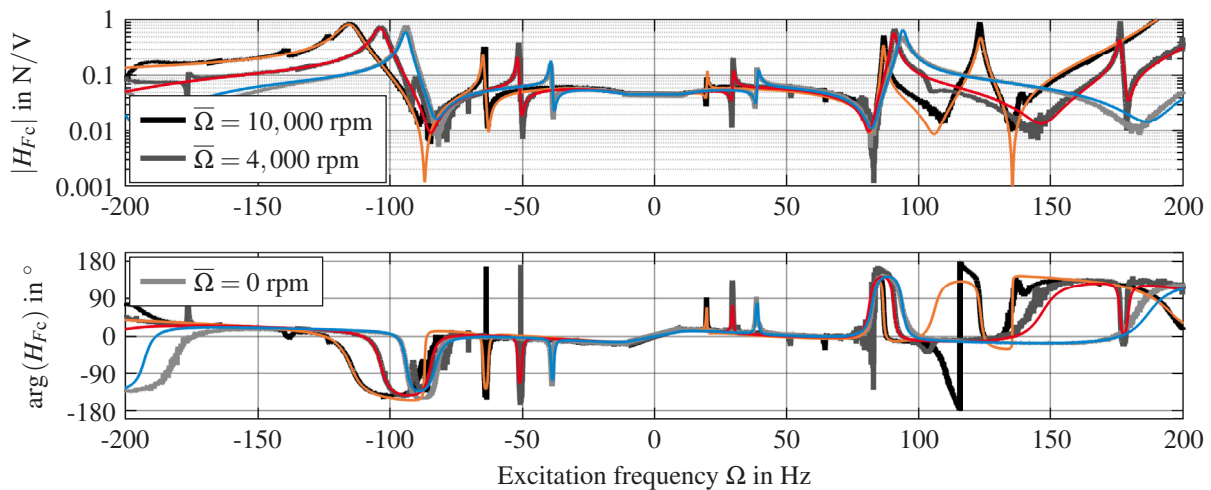


Fig. 4. Estimated closed-loop transfer function H_{Fc} for three stationary rotor speeds together with the fitted modal model with a linear function for the modal residuum $V_{F1} = v_0 + v_1\bar{\Omega}$. The blue, red and orange line correspond to the fits at 0, 4000 and 10 000 rpm respectively. Negative frequencies correspond to the forward whirl and positive frequencies to the backward whirl since the rotor rotates into the negative x -direction. The legends are shared among both plots

of the simple numerator of the trial function (5). The fit can be improved significantly by using a linear function for the modal residual $V_{F1} = v_0 + v_1\bar{\Omega}$ which can compensate some simplifications as shown in Fig. 4. However, since there is no reasoning for this approach, it will be discarded and not applied in

this paper due to possible overfitting. Experimental results of the FxLMS using a model with constant or linear modal residual show no significant differences since a phase mismatch of $\pm 40^\circ$ has no significant influence on the performance of the FxLMS [13].

4. CONTROLLER DESIGN

In accordance with the literature review, the control approach which yields the best results for unbalance vibration elimination is a combination of a feedback controller and an adaptive feedforward controller. An IFF-controller

$$H_{\text{IFF}} = \frac{\mathcal{F}\{U_c\}}{\mathcal{F}\{F_L\}} = -\frac{k_{\text{IFF}}}{i\Omega + \gamma_{\text{IFF}} k_{\text{IFF}}} \quad (7)$$

can be used to increase the damping of the system where k_{IFF} is the amplification factor and γ_{IFF} the forgetting factor. The controller integrates the force over time resulting in active damping. At this point it is crucial that a high-pass filter is used to filter out the static forces which cannot be eliminated and cause the closed-loop system to be unstable for $\gamma_{\text{IFF}} = 0$. For $\gamma_{\text{IFF}} > 0$ the system is in theory stable but the controller still produces a useless controller output which might hinder the feedback at other frequencies. The closed-loop transfer function of the system with an IFF controller is given by

$$H_{F_c} = \frac{H_F}{1 - H_F H_{\text{IFF}}} \quad (8)$$

and has been identified throughout the experimental modal analysis in the section before.

Of more importance is the choice of the adaptive feedforward control which will be explained more in detail. A well-researched control algorithm of this class is the least-mean-squares (LMS) algorithm [14, 13]. The algorithm explained in the following is for a single-input-single-output system but can be extended to a multi-input-multi-output system without loss of generality. The objective is to eliminate the bearing force F_L of Bearing 1 with the actuator voltage U_a . The algorithm is based on minimizing the squared control error [13]. In this paper we chose to minimize the bearing force by using the complex amplitude of the actuator voltage \hat{U}_a in the fashion

$$\min_{\hat{U}_a} (F_L^* F_L) \quad \text{with } F_L = \hat{F}_L e^{i\varphi}, U_a = \hat{U}_a e^{i\varphi} \quad (9)$$

where the operator $*$ represents the complex conjugate, φ the reference angle, which is in our case equal to the instantaneous rotor angle, and \hat{F}_L the complex amplitude of the bearing force. Note that we use the closed-loop transfer function assuming that IFF is used. The minimum is given when the first derivative of the squared control error in respect to the actuator voltage amplitude equals zero

$$\begin{aligned} \nabla_U &= \frac{d}{d\hat{U}_a} (F_L^* F_L) = F_L^* H_{F_c} e^{i\varphi} \stackrel{!}{=} 0 \\ \text{with } \nabla_U &= \frac{1}{2} \frac{d}{d\Re\{\hat{U}_a\}} - \frac{1}{2} i \frac{d}{d\Im\{\hat{U}_a\}}. \end{aligned} \quad (10)$$

The optimal voltage amplitudes cannot be directly computed since F_L^* is a function of the unknown unbalance. However, the minimum can be reached by following the gradient ∇_U step by step in the negative conjugate complex direction yielding the discrete update equation

$$\begin{aligned} \hat{U}_a[n+1] &= (1 - \gamma\Delta t) \hat{U}_a[n] - \alpha\Delta t H_{F_c}^*[n] F_L[n] e^{-i\varphi[n]}, \\ U_a[n+1] &= \hat{U}_a[n+1] e^{i\varphi[n]}, \end{aligned} \quad (11)$$

where α is the real valued step size and Δt the sample time. Note that this approach automatically yields the update equation of the FxLMS since the time signals are complex. Thus, we will refer to it as the FxLMS instead of just LMS. Furthermore, we can filter the complex time signal directly with the transfer function. A forgetting factor γ is introduced, analogous to IFF, to increase the stability [13] since a practical application will always have remaining vibrations.

The convergence of the algorithm is depending on the quality of the model \hat{H}_{F_c} of the closed-loop transfer function H_{F_c} and the step-size α . The FxLMS will converge for limited step sizes if the maximum phase error of the model \hat{H}_{F_c} is less than $\pm 90^\circ$ [13]. A phase error less than $\pm 40^\circ$ does not cause a significant slower convergence [13]. The maximum step size α depends on the magnitude of the transfer function $|H_F|$ at the current operating point and is proportional to $1/|H_{F_c}|^2$ [15]. For practical applications, a safety margin δ is used in the form

$$\alpha = \frac{\alpha_0}{\delta + |H_{F_c}|^2} \quad \text{with } \delta > 0, \alpha_0 \in (0, 2) \quad (12)$$

which avoids a too large step size in zeros of H_{F_c} [15]. The convergence of the algorithm is also strongly depending on the presence of other uncorrelated frequencies [16]. For example, if we want to eliminate the unbalance forces which frequency is proportional to the rotor speed $\bar{\Omega}$, a present disturbance with twice the frequency will reduce the convergence speed. Using an additional transformation can remedy this, yielding the transform-domain LMS [16]. However, since approximately only one frequency is present at a time, it is unnecessary to take such measures. Thus, the overall discrete update equation for a combination of IFF and the FxLMS, which we refer to as model-based controller, is given by

$$\begin{aligned} u_{\text{IFF}}[n+1] &= (1 - \gamma_{\text{IFF}} k_{\text{IFF}} \Delta t) u_{\text{IFF}}[n] - k_{\text{IFF}} \Delta t F_L[n], \\ u_{\text{FxLMS}}^+[n+1] &= (1 - \gamma\Delta t) u_{\text{FxLMS}}^+[n] \\ &\quad - \alpha_0 \Delta t \frac{H_{F_c}^*(\bar{\Omega}[n])}{\delta + |H_{F_c}(\bar{\Omega}[n])|^2} F_L[n] e^{-i\varphi[n]}, \\ u_{\text{FxLMS}}^-[n+1] &= (1 - \gamma\Delta t) u_{\text{FxLMS}}^-[n] \\ &\quad - \alpha_0 \Delta t \frac{H_{F_c}^*(-\bar{\Omega}[n])}{\delta + |H_{F_c}(-\bar{\Omega}[n])|^2} F_L[n] e^{+i\varphi[n]}, \\ U_a[n+1] &= u_{\text{IFF}}[n+1] + u_{\text{FxLMS}}^+[n+1] e^{+i\varphi[n]} \\ &\quad + u_{\text{FxLMS}}^-[n+1] e^{-i\varphi[n]}. \end{aligned} \quad (13)$$

A model-free control approach can now be designed using the prior mentioned convergences and stability criteria. The actuator and force sensor of the identified system are approximately collocated which means that zeros and poles always appear in according pairs. This causes the phase within the operating range to be approximately between 0 and 180° for the

backward whirl ($\Omega > 0$) and between 0 and -180° for the forward whirl ($\Omega < 0$). This would always be true if the system comprises only poles and zeros with a negative real-part and has no delay time. Assuming this to be true, we can define a model of the secondary path \tilde{H}_F which fulfills the convergence criteria of the FxLMS. Choosing the models

$$\tilde{H}_{F_c}^+ = i \quad \text{and} \quad \tilde{H}_{F_c}^- = -i \quad (14)$$

for the backward whirl, indicated by plus, and the forward whirl, indicated by minus, respectively, results in a phase mismatch which is no bigger than $\pm 90^\circ$ since the phase of the secondary path model is constant $+90^\circ$ for positive frequencies corresponding to the backward whirl and -90° for negative frequencies corresponding to the forward whirl. The maximum step size α is depending on the maximum value of the transfer function H_{F_c} within the operating range as described in Eq. (12). Thus, an undamped system can never be controlled in resonances using the FxLMS only since $H_{F_c} \rightarrow \infty$ and thus $\alpha \rightarrow 0$. Damping is required to control such a system which can be provided by using IFF since the system is approximately collocated. The presence of damping also causes the phase to never actually reach the values -180° , 0° and 180° for either backward or forward whirl respectively for $\Omega \neq 0$. This allows a convergences of the FxLMS since the phase mismatch never equals either $\pm 90^\circ$ because the algorithm will never converge for a phase mismatch of exactly $\pm 90^\circ$. Thus, damping is necessary for the implementation even aside the resonances. The discrete update equation for a combination of IFF and the model-free FxLMS based on Eq. (11), which we will refer to as model-free controller, is given by

$$\begin{aligned} u_{\text{IFF}}[n+1] &= (1 - \gamma_{\text{IFF}} k_{\text{IFF}} \Delta t) u_{\text{IFF}}[n] - k_{\text{IFF}} \Delta t F_L[n], \\ u_{\text{FxLMS}}^+[n+1] &= (1 - \gamma \Delta t) u_{\text{FxLMS}}^+[n] + i\alpha_0 \Delta t F_L[n] e^{-i\varphi[n]}, \\ u_{\text{FxLMS}}^-[n+1] &= (1 - \gamma \Delta t) u_{\text{FxLMS}}^-[n] - i\alpha_0 \Delta t F_L[n] e^{+i\varphi[n]}, \\ U_a[n+1] &= u_{\text{IFF}}[n+1] + u_{\text{FxLMS}}^+[n+1] e^{+i\varphi[n]} \\ &\quad + u_{\text{FxLMS}}^-[n+1] e^{-i\varphi[n]}. \end{aligned} \quad (15)$$

Note that this algorithm is the same algorithm as the one Heindel proposed in [11]. The delay-time can and will destabilize the proposed controller if the delay-time or the excitation frequency is too high since the phase will leave the assumed $\pm 90^\circ$ window as can be seen in Fig. 3. This can be remedied by using the models

$$\tilde{H}_{F_c}^+ = i e^{-i\Omega\tau} \quad \text{and} \quad \tilde{H}_{F_c}^- = -i e^{i\Omega\tau} \quad (16)$$

which require the knowledge of the delay-time τ making the controller not completely model-free anymore. An extension to further harmonics is possible by using different reference angles and adding them to the controller output respectively for forward and backward whirl. Only the rotor synchronous unbalance excitation for forward and backward whirl will be considered in this paper.

The controller has a limited step size α which has to be identified by trial and error for a practical implementation. The step size is limited by the maximum value of the closed-loop transfer function and is constant for the whole operating range. This causes a relative small step size aside the resonances causing a slower convergence than the model-based controller which uses the models $\tilde{H}_{F_c}^+ = H_{F_c}^+$ and $\tilde{H}_{F_c}^- = H_{F_c}^-$. The phase error in most areas aside the resonances and zeros is greater than $\pm 40^\circ$ causing the algorithm to converge even slower. Thus, we can expect a fast convergence in the resonances but a slow one aside from them. Furthermore, a delay time will cause the controller to be unstable for too high frequencies which can be remedied by consideration of the delay-time. An operation in a zero can lead to high output voltages U_a which need to be limited by the forgetting factor γ . If the closed-loop system without adaptive feedforward shows zeros with a positive real-part, which is the case for the zero at 120 Hz at a rotor speed of 10 000 rpm in Fig. 3, the controller will become unstable in this region if the forgetting factor γ is too small. Since there is a limit for the maximum amplification factor k_{IFF} for practical implementation, which also limits the active damping, the system will become unstable for too high rotor speeds if internal damping is present. Thus, a model-free control which always converges is not possible because of delay-time and internal damping.

5. EXPERIMENTAL RESULTS

The test-rig in Fig. 1 is used for a comparison of the model-free controller from Eq. (15) and the model-based algorithm from Eq. (13). The model-free controller comprises IFF and the FxLMS which uses the $\pm 90^\circ$ model from Eq. (14). Thus, it does not consider the delay time. The model-based controller is also combination of IFF and the FxLMS but uses the prior identified modal model comprising delay time and the system dynamics including internal damping. Furthermore, the model-based controller uses a normalized step-size.

The rotor is elastically balanced for the first and second forward whirl resonance with a remaining rigid rotor unbalance of ca. 125 g mm on Disc 1 and 242 g mm on Disc 2 at 1000 rpm. The unbalance is mainly caused by the shaft runout of the rotor which has a radius of ca. 0.05 mm at both discs measured at 100 rpm. Rotor run-ups are used for comparison of the controller performances. However, since the rotor shows internal damping and becomes unstable after the second forward whirl resonance at 110 Hz, a passive run-up cannot be used. Figure 5 shows a passive run-up with 400 rpm/s where the bearing force increases exponentially. This instability was not predictable by the modal model, probably because of the simple approach or non-linearities. The rotor has been stopped and IFF was activated causing the vibrations to decrease in order to prevent damage. The envelop of the signal is used in the following for comparison of the controller performances. The envelop is computed by using order-tracking adding the absolute value of the amplitudes of the orders -2 , -1 , 1 and 2 together, which are the multiples of the rotor speed. The sliding discrete Fourier-transformation with a changing window length which always

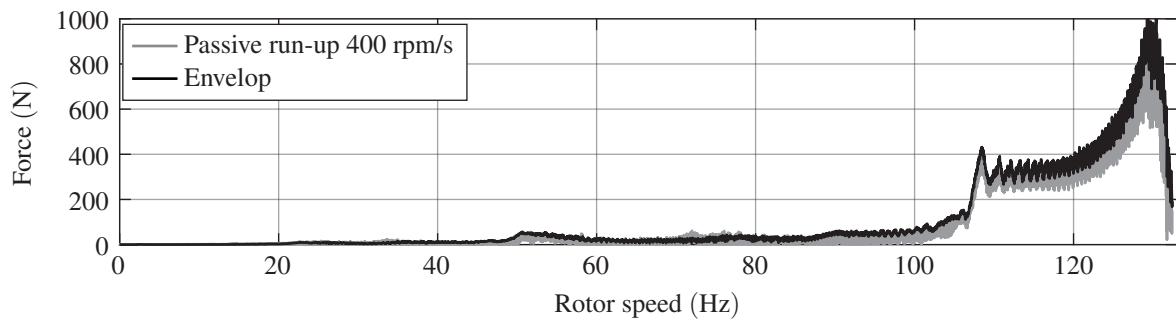


Fig. 5. Absolute force of Bearing 1 from a passive run-up of the rotor with 400 rpm/s. The rotor was stopped at ca. 130 Hz and IFF was activated. Shown is also the envelop of the signal

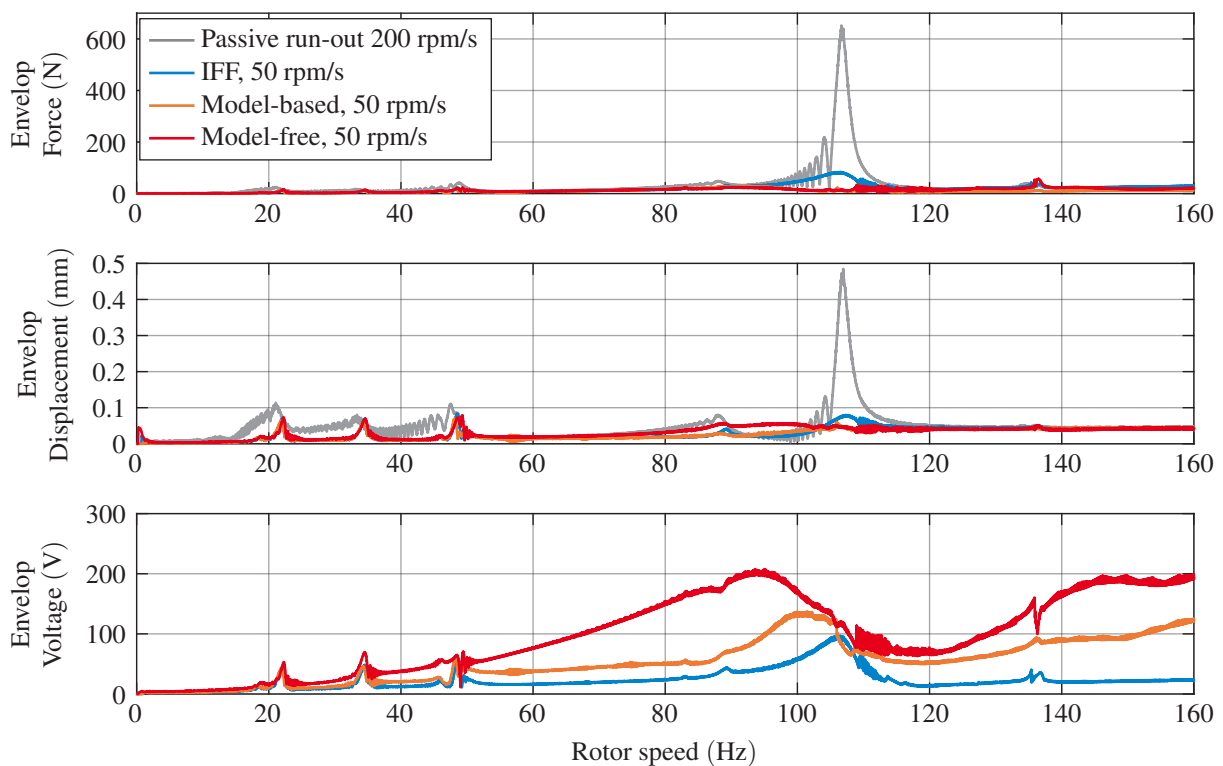


Fig. 6. Active control results for three different controllers for rotor run-ups and a passive rotor run-out for comparison. The control objective was to reduce the force of Bearing 1. Depicted are the envelopes of the force of Bearing 1, the displacement of Disc 1 and the voltage of the active plane. The legend is shared among all plots. The model-free controller uses the update equation Eq. (15) and the model-based controller Eq. (13)

covers a full rotor rotation was used to extract the amplitudes as described in [17].

Figure 6 shows the results of IFF alone and in combination with the model-free and model-based controller. The reference angle φ was extracted with an incremental encoder. The control parameters were $k_{\text{IFF}} = 800$, $\gamma_{\text{IFF}} = \gamma = \delta = 0.1$ and $\alpha_0 = 1$ with a sampling rate of 6000 Hz. IFF is reducing the amplitudes of the second resonance significantly but still keeps remaining vibrations. Using the derived model-free controller or the model-based controller allows a nearly complete elimination of the second resonance at 110 Hz where both controllers show the same performance. However, it can be seen that the model-free

control approach has a significant higher control output when the rotor speed is not close to a resonance, for example in the range between 50 and 90 Hz as well as above 120 Hz. This is caused by a phase mismatch of the model \tilde{H}_{Fc}^+ which is bigger than 90° because the phase of the transfer function is above 0° which can be seen in Fig. 3. This causes the model-free controller to diverge causing the displacements to increase. The divergence is slow since the phase mismatch is close to 90° where an exact phase mismatch of 90° has no influence on the bearing forces but can increase the displacements of the rotor. The divergence is also limited by the forgetting factor γ . The model-based controller keeps a nearly constant actuator voltage

in the area between 50 and 90 Hz suggesting that the increasing voltage of the model-free controller is caused by the not sufficient model \hat{H}_{Fc}^+ . Furthermore, the presence of a zero in this area causes the voltage to increase. This is prevented in case of the model-based controller throughout the use of a normalized step-size with a sufficiently high safety margin in combination with the forgetting factor γ .

The first three peaks at 22 Hz, 35 Hz and 49 Hz belong to the first forward whirl resonance excited by the second order, the first backward whirl resonance excited by the negative first order and first forward whirl resonance excited by the first order, which corresponds to the unbalance excitation, respectively. Thus, the test-rig has non-isotropic bearings which excite the backward whirl. However, the assumption of an isotropic and isotropic bearing made in Section 2 are still sufficient for the model of the controller since the model-based controller did converge at all rotor speeds. These resonances are not significantly reduced by the control. The reason therefore is that resonances nearly only excite the disc displacements but not the bearing forces. Since the controllers only use the bearing forces, they cannot generate a sufficient controller output to eliminate the resonances. Furthermore, the rotor centres itself after passing the second forward whirl resonance as can be seen at rotor speeds higher than 120 Hz. The remaining displacement is ca. 0.04 mm which is close to the runout of 0.05 mm and not in conflict with the control objective either.

6. CONCLUSION

A gyroscopic rotor system with active piezoelectric bearings has been modelled and identified throughout experimental modal analysis. A simple trial function has been deployed which yields good results. The trial function is based on the separation of the eigenvalues into a real and imaginary part, yielding the poles of the system, in order to fit the model to experimental data. A model-free control based on the FxLMS in combination with IFF has been designed for a collocated actuator sensor pair. The stability and convergence of the controller is limited by internal damping and the delay-time which causes the phase mismatch to increase with rising excitation frequency. The delay-time has to be included into the algorithm for improving the stability making the controller no longer completely model-free. The model-free controller shows a similar performance as the model-based controller near the resonances but diverges aside the resonances which can be limited with a forgetting factor. Both controllers were able to stabilize the unstable system which was induced by internal damping. Thus, a model-free control approach which can theoretically eliminate the bearing forces at all rotor speeds is not feasible in a real system because of the delay-time.

ACKNOWLEDGEMENTS

Funded by the Deutsche Forschungsgemeinschaft (DFG, German Research Foundation) – 435227428. The used measurement data in this paper is available here: [18].

REFERENCES

- [1] A.B. Palazzolo, R.R. Lin, R.M. Alexander, A.F. Kascak, and J. Montague, “Test and theory for piezoelectric actuator-active vibration control of rotating machinery,” *J. Vib. Acoust.*, vol. 113, no. 2, 1991. doi: 10.1115/1.2930165.
- [2] R. Köhler, C. Kaletsch, M. Marszolek, and S. Rinderknecht, “Active vibration damping of engine rotor considering piezoelectric self heating effects,” in *International Symposium on Air Breathing Engines 2011 (ISABE 2011)*, Gothenburg, Sep. 2011.
- [3] M. Borsdorf, R.S. Schittenhelm, and S. Rinderknecht, “Vibration reduction of a turbofan engine high pressure rotor with piezoelectric stack actuators,” in *Proceedings of the International Symposium on Air Breathing Engines 2013 (ISABE 2013)*, Busan, 2013.
- [4] R.C. Simões, V. Steffen, J. Der Hagopian, and J. Mahfoud, “Modal active vibration control of a rotor using piezoelectric stack actuators,” *J. Vib. Control*, vol. 13, no. 1, pp. 45–64, Jan. 2007. doi: 10.1177/1077546306070227.
- [5] B. Riemann, M.A. Sehr, R.S. Schittenhelm, and S. Rinderknecht, “Robust control of flexible high-speed rotors via mixed uncertainties,” in *2013 European Control Conference (ECC)*. Zürich: IEEE, Jul. 2013, pp. 2343–2350. doi: 10.23919/ECC.2013.6669786.
- [6] F.B. Becker, M.A. Sehr, and S. Rinderknecht, “Vibration isolation for parameter-varying rotor systems using piezoelectric actuators and gain-scheduled control,” *J. Intell. Mater. Syst. Struct.*, vol. 28, no. 16, pp. 2286–2297, Sep. 2017. doi: 10.1177/1045389X17689933.
- [7] M. Li, T.C. Lim, and W.S. Shepard, “Modeling active vibration control of a geared rotor system,” *Smart Mater. Struct.*, vol. 13, no. 3, pp. 449–458, Jun. 2004. doi: 10.1088/0964-1726/13/3/001.
- [8] Y. Suzuki and Y. Kagawa, “Vibration control and sinusoidal external force estimation of a flexible shaft using piezoelectric actuators,” *Smart Mater. Struct.*, vol. 21, no. 12, Dec. 2012. doi: 10.1088/0964-1726/21/12/125006.
- [9] O. Lindenborn, B. Hasch, D. Peters, and R. Nordmann, “Vibration reduction and isolation of a rotor in an actively supported bearing using piezoelectric actuators and the FXLMS algorithm,” in *9th International Conference on Vibrations in Rotating Machinery*, Exeter, Sep. 2008.
- [10] R.S. Schittenhelm, S. Bevern, and B. Riemann, “Aktive Schwingungsminderung an einem gyroskopiebehalteten Rotorsystem mittels des FxLMS-Algorithmus,” in *SIRM 2013 – 10. Internationale Tagung Schwingungen in rotierenden Maschinen*, Berlin, Deutschland, Feb. 2013.
- [11] S. Heindel, P.C. Müller, and S. Rinderknecht, “Unbalance and resonance elimination with active bearings on general rotors,” *J. Sound Vib.*, vol. 431, pp. 422–440, Sep. 2018. doi: 10.1016/j.jsv.2017.07.048.
- [12] B. Vervisch, K. Stockman, and M. Loccufier, “A modal model for the experimental prediction of the stability threshold speed,” *Appl. Math. Modell.*, vol. 60, pp. 320–332, Aug. 2018. doi: 10.1016/j.apm.2018.03.020.
- [13] S. Kuo and D. Morgan, “Active noise control: a tutorial review,” *Proc. IEEE*, vol. 87, no. 6, pp. 943–975, Jun. 1999. doi: 10.1109/5.763310.
- [14] J. Jiang and Y. Li, “Review of active noise control techniques with emphasis on sound quality enhancement,” *Appl. Acoust.*, vol. 136, pp. 139–148, Jul. 2018. doi: 10.1016/j.apacoust.2018.02.021.

- [15] L.P. de Oliveira, B. Stallaert, K. Janssens, H. Van der Auweraer, P. Sas, and W. Desmet, “NEX-LMS: A novel adaptive control scheme for harmonic sound quality control,” *Mech. Syst. Signal Process.*, vol. 24, no. 6, pp. 1727–1738, Aug. 2010. doi: [10.1016/j.ymssp.2010.01.004](https://doi.org/10.1016/j.ymssp.2010.01.004).
- [16] S.S. Narayan, A.M. Peterson, and M.J. Narasimha, “Transform domain LMS algorithm,” *IEEE Trans. Acoust. Speech Signal Process.*, vol. 31, no. 3, pp. 609–615, Jun. 1983.
- [17] J. Jungblut, D.F. Plöger, P. Zech, and S. Rinderknecht, “Order tracking based least mean squares algorithm,” in *Proceedings of 8th IFAC Symposium on Mechatronic Systems MECHATRONICS 2019*, Vienna, Sep. 2019, pp. 465–470.
- [18] J. Jungblut, C. Fischer, and S. Rinderknecht, “Supplementary data: Active vibration control of a gyroscopic rotor using experimental modal analysis,” 2020. [Online]. doi: [10.48328/tudata-lib-572](https://doi.org/10.48328/tudata-lib-572).